



# CHORUS

This is the accepted manuscript made available via CHORUS. The article has been published as:

## Searching for crystal-ice domains in amorphous ices

Fausto Martelli, Nicolas Giovambattista, Salvatore Torquato, and Roberto Car

Phys. Rev. Materials **2**, 075601 — Published 2 July 2018

DOI: [10.1103/PhysRevMaterials.2.075601](https://doi.org/10.1103/PhysRevMaterials.2.075601)

# Searching for crystal-ice domains in amorphous ices

Fausto Martelli<sup>1,2,\*</sup>, Nicolas Giovambattista<sup>3,4</sup>, Salvatore Torquato<sup>2</sup>, Roberto Car<sup>2</sup>

<sup>1</sup>*IBM Research, Hartree Centre,*

*Daresbury, WA4 4AD, United Kingdom*

<sup>2</sup>*Department of Chemistry, Princeton University,  
Princeton, New Jersey 08544, USA*

<sup>3</sup>*Department of Physics,  
Brooklyn College of the City University of New York,  
Brooklyn, New York 11210, USA*

<sup>4</sup>*The Graduate Center of the City University of New York,  
New York, New York 10016, USA*

\* *Corresponding author: fausto.martelli@ibm.com*

We employ classical molecular dynamics simulations to investigate the molecular-level structure of water during the isothermal compression of hexagonal ice (*Ih*) and low-density amorphous (LDA) ice at low temperatures. In both cases, the system transforms to high-density amorphous ice (HDA) via a first-order-like phase transition. We employ a sensitive local order metric (LOM) [Martelli *et. al.*, *Phys. Rev. B*, **97**, 064105 (2018)], that can discriminate among different crystalline and non crystalline ice structures and is based on the positions of the oxygen atoms in the first and/or second hydration shell. Our results confirm that LDA and HDA are indeed amorphous, i.e., they lack of polydispersed ice domains. Interestingly, HDA contains a small number of domains that are reminiscent of the unit cell of ice IV, although the hydrogen-bond network (HBN) of these domains differ from the HBN of ice IV. The presence of ice IV-like domains provides some support to the hypothesis that HDA could be the result of a detour on the HBN rearrangement along the *Ih*-to-ice IV pressure induced transformation. Both nonequilibrium LDA-to-HDA and *Ih*-to-HDA transformations are two-steps processes where a small distortion of the HBN first occurs at low pressures and then, a sudden, extensive re-arrangement of hydrogen bonds at the corresponding transformation pressure follows. Interestingly, the *Ih*-to-HDA and LDA-to-HDA transformations occur when LDA and *Ih* have similar local order, as quantified by the site-averaged LOMs. Since *Ih* has a perfect tetrahedral HBN, while LDA does not, it follows that higher pressures are needed to transform *Ih* into HDA than that for the conversion of LDA to HDA. In correspondence with both first-order-like phase transitions, the samples are composed of a large HDA cluster that percolates within the *Ih*/LDA samples.

Our results shed light on the debated structural properties of amorphous ices and indicate that the kinetics of the *Ih*-to-HDA and LDA-to-HDA transformations require an in depth inspection of the underlying HBN. Such investigation is currently ongoing.

## I. INTRODUCTION

At deeply supercooled conditions, water exhibits polyamorphism, i.e., it exists in more than one amorphous solid state. The most common forms of glassy water are the low-density amorphous (LDA) and the high-density amorphous (HDA) ice<sup>1-6</sup>. LDA is likely the most abundant form of ice in the universe and can be produced, for example, by rapid quenching of liquid water at atmospheric pressure<sup>7</sup>. The LDA that is thought to exist in space forms by condensation of water from the gas phase onto cold surfaces<sup>8,9</sup>. HDA can be produced, for example, by pressure induced amorphization (PIA) of hexagonal ice (*Ih*) or by isothermal compression of LDA<sup>10-13</sup>. Remarkably, LDA and HDA can be interconverted by isothermal compression/decompression at  $T = 130 - 140$  K<sup>10,14,15</sup> and by isobaric heating at different pressures<sup>14,16,17</sup>. A third form of glassy water, a very high-density amorphous ice (VHDA), has been identified at very high pressures<sup>18</sup>. We note that experiments show that LDA and HDA can be separated

into subfamilies of amorphous structures, e.g., LDA<sub>I</sub> and LDA<sub>II</sub> for LDA<sup>19</sup>, and unannealed HDA (uHDA) and expanded HDA (eHDA) for the case of HDA<sup>5,6,20,21</sup>. However, this distinction is less clear in computer simulations and, therefore, we refer to glassy water as either LDA or HDA.

At small length scales, LDA and HDA are structurally very different. LDA has well-separated first and second hydration shells, with nearest-neighbors arranged in a tetrahedral-like local structure. In this regard, the structure of LDA is reminiscent of the local structure of *Ih*. By contrast, HDA has interstitial molecules populating the space between the first and the second hydration shells, thus acquiring distorted local configurations similar to liquid water configurations at ambient conditions<sup>16,22-26</sup>. LDA and HDA also differ in terms of the hydrogen-bond network (HBN). The HBN of LDA is dominated by 5-, 6-, and 7-fold rings, in contrast to HDA, whose HBN includes a significant fraction of longer member rings to accommodate the larger density of the system ( $\sim 20 - 25\%$  larger than LDA)<sup>27</sup>. Despite these local structural differences, at large length scales the two glass forms are

nearly hyperuniform, i.e., they possess similar degree of suppression of large-scale density fluctuations, indicating that they should possess similar large-scale structures and large-scale translational order<sup>28</sup>.

LDA and HDA were discovered more than 30 years ago<sup>1</sup>. Yet, the nature of LDA and HDA, and the associated LDA-to-HDA first-order-like phase transition, remain highly debated. It has been suggested that LDA and HDA are thermodynamically connected with the liquid, e.g., by isobaric cooling/heating<sup>10</sup>. Elsewhere, HDA was interpreted to be a collapsed HBN of water molecules, unrelated to the liquid state<sup>29–31</sup>. It has also been suggested that HDA may contain nanometer-scale ice domains. After all, HDA transforms to ice IV at very high pressure<sup>32,33</sup> and it can be formed by compression of *Ih*. Unfortunately, experimental studies that focus on the structure of LDA and HDA at intermediate length scales are challenging<sup>6</sup>. Computer simulation studies that describe the structure of LDA and HDA, especially the search for the presence of ice-like domains, are rare.

In this article, we perform out-of-equilibrium classical MD simulations to study the structural order during the *Ih*-to-HDA and LDA-to-HDA transformations; in particular, we look for traces of crystalline domains during these processes. We will refer to the HDA produced upon compression of *Ih* as  $\text{HDA}_{Ih}$ , and to the HDA obtained upon compression of LDA as  $\text{HDA}_{LDA}$ . We probe the short- and intermediate-range order during these transformations using a recently developed local order metric (LOM). The LOM measures the degree of order present in the neighborhood of an atomic or molecular site in a condensed medium<sup>34</sup>. The LOM is endowed with a high-resolving power<sup>34–36</sup> and allows one to look for specific ordered domains defined by the location of selected atoms (e.g., water oxygens) in a given reference structure. Typically, the reference structure is taken to be the local structure of a perfect crystalline phase.

We have looked for signatures of ices *Ih*, cubic (Ic), II, III, IV, V, VI, and VII, in LDA and HDA. According to our analysis, both amorphous ices lack polydispersed ordered crystalline domains. However, we find that the oxygens of few water molecules in HDA are arranged as in the unit cell of ice IV. This observation provides support to the picture proposed in Ref.<sup>37</sup>, where the collapse of the HBN of *Ih* occurring upon isothermal compression does not lead to ice IV, but to HDA, hence considered a 'derailed' state along the *Ih*-to-ice IV pathway. Our observation is also consistent with the transformation of HDA to ice IV reported in experiments at very high pressures<sup>32,33</sup>. On the other hand, we also find that the HBN connecting the water molecules in these ice IV-like domains in HDA *differs* from the HBN in the unit cell of ice IV.

Our analysis indicates that the *Ih*-to-HDA transformation is a two-step process in which, first, compression causes a continuous distortion of the ordered HBN of *Ih*. This continuous distortion of the HBN is then followed

by a sudden extensive rearrangement of the HBN that occurs in correspondence with the *Ih*-to-HDA first-order-like phase transition. A similar two-step process occurs during the LDA-to-HDA transformation. In this case, however, although LDA and *Ih* acquire similar tetrahedral configurations, the LDA-to-HDA transformation is milder than the *Ih*-to-HDA transformation, and it occurs at lower pressures. We notice that the second hydration shell in *Ih* is well ordered. Conversely, the second hydration shell in LDA describes an 'open cage' with a disordered HBN and, therefore, is less rigid. Hence, we relate the lower transformation pressure in LDA, relative to *Ih*, to the lower rigidity of the second hydration shell in LDA compared to *Ih*. We complement our analysis by performing a clustering analysis of local environments at different pressures and show that both LDA-to-HDA and *Ih*-to-HDA transformations are reminiscent to spinodal decompositions, without nucleation and growth of HDA within LDA/*Ih*.

The article is organized as follows. In Section II, we provide a brief definition of the LOM employed in this work. In Secs. III A and III B, we discuss the short- and the intermediate-range order, respectively, in both LDA and HDA. In Section III C, we discuss the spatial aggregation (clusters) of LDA-, HDA-, and *Ih*-like molecules during the LDA-to-HDA and *Ih*-to-HDA transformations. Conclusions and final remarks are presented in Sec. IV.

## II. THE LOCAL ORDER METRIC

In this section, we briefly describe the local order metric employed in this work. The details of the numerical algorithm can be found in Ref.<sup>34</sup>. The local environment of an atomic site  $j$  in a snapshot of a molecular dynamics or Monte Carlo simulation defines a local pattern formed by  $M$  neighboring sites. Typically these include the first and/or the second neighbors of the site  $j$ . There are  $N$  local patterns, one for each atomic site  $j$  in the system. The local reference structure is the set of the same  $M$  neighboring sites in an ideal lattice of choice, the spatial scale of which is fixed by setting its nearest neighbor distance equal to  $d$ , the average equilibrium value in the system of interest. For a given orientation of the reference structure and a given permutation  $\mathcal{P}$  of the pattern indices, we define the LOM  $S(j)$  as the maximum overlap between pattern and reference structure in the  $j$  neighborhood by:

$$S(j) = \max_{\theta, \phi, \psi; \mathcal{P}} \left\{ \prod_{i=1}^M \exp \left( - \frac{|\mathbf{P}_{i\mathcal{P}}^j - \mathbf{A}^j \mathbf{R}_i^j|^2}{2\sigma^2 M} \right) \right\} \quad (1)$$

Where  $\theta, \phi$  and  $\psi$  are Euler angles,  $\mathbf{P}_{i\mathcal{P}}^j$  and  $\mathbf{R}_i^j$  are the pattern and the reference position vectors in the laboratory frame of the  $M$  neighbors of site  $j$ , respectively,

and  $\mathbf{A}^j$  is an arbitrary rotation matrix about the pattern centroid. The parameter  $\sigma$  controls the spread of the Gaussian functions ( $\sigma = d/4$  in this work, where  $d$  is the characteristic length of the local pattern). The LOM satisfies the inequalities  $0 \lesssim S(j) \leq 1$ . The two limits correspond, respectively, to a local pattern with randomly distributed points ( $S(j) \rightarrow 0$ ) and to an ordered local pattern matching perfectly the reference ( $S(j) \rightarrow 1$ ). We also define a global order parameters based on  $S(j)$ , as the average score function  $S$ :

$$S = \frac{1}{N} \sum_{j=1}^N S(j) \quad (2)$$

To improve statistics, the score functions are also averaged over 10 independent (LDA-to-HDA and *Ih*-to-HDA) trajectories.

### III. RESULTS

Our study is based on classical molecular dynamics simulations of a system of  $N = 8192$  water molecules described by the classical TIP4P/2005 interaction potential<sup>38</sup>. This water model is able to reproduce relatively well the structures of LDA and HDA at low temperatures<sup>26</sup>. Computer simulations details and a description of the protocols employed in this work are provided in Ref.<sup>39</sup>. Briefly, we prepare LDA by cooling an equilibrium liquid from 240 K to 80 K, with a cooling rate of 1 K/ns. HDA is obtained by isothermal compression of *Ih* and LDA at  $T = 80$  K. During the compression of *Ih* and LDA, the pressure is increased from ambient to 3.0 GPa at a pace of 0.01 GPa/ns. For the water model considered, at the present cooling and compression rates, the *Ih*-to-HDA transformation occurs at  $p = 1.35$  GPa, while the LDA-to-HDA transformation occurs at  $0.83 \lesssim p \lesssim 0.93$  GPa<sup>39</sup>. All results reported in this work are averaged over 10 independent trajectories.

#### A. Short-range order: local tetrahedrality

In this section, we discuss the local structure of water during the LDA-to-HDA and *Ih*-to-HDA transformation at the level of the first hydration shell. Experiments and computer simulations indicate that the local structure of *Ih* and LDA is tetrahedral, i.e., a given molecule is located at the center of a tetrahedron and its four nearest-neighbors are roughly located at the corner of such a tetrahedron. Therefore, in order to probe the short-range order of water during the LDA-to-HDA and *Ih*-to-HDA transformations, we consider a LOM defined using, as a reference structure, a regular tetrahedron. The resulting score function,  $S_{th}$ , is shown in Fig. 1 for the compression of *Ih* (black circles) and LDA (red squares). At low applied pressures, both *Ih* and LDA acquire high values

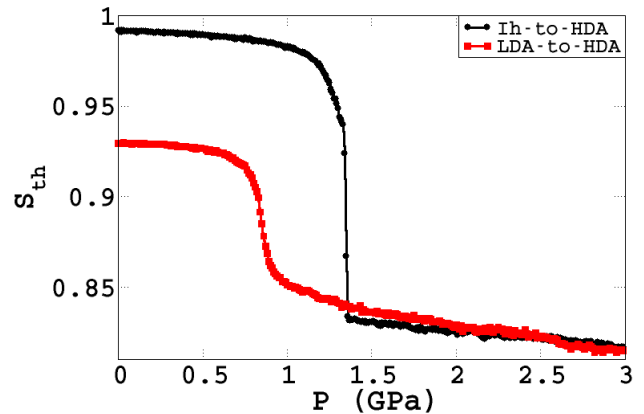


FIG. 1: Local tetrahedrality during the *Ih*-to-HDA (black circles) and LDA-to-HDA (red squares) transformations.  $S_{th}$  is the score function defined using a regular tetrahedron as a reference structure. In both transformations, compression at low pressures leads to a continuous decrease in local tetrahedrality. The sudden jump in  $S_{th}$  at  $p \sim 0.83$  GPa (LDA) and  $p \sim 1.36$  GPa (*Ih*) coincides with the sharp transformation of the system to HDA<sup>39</sup>.

of  $S_{th}$ , reflecting the nearly perfect regular tetrahedrality of *Ih* and LDA. Upon compressing the samples,  $S_{th}$  slightly decreases as the local tetrahedral structures get more and more distorted. The transformation of LDA and *Ih* to HDA occur, respectively, at  $0.83 \lesssim p \lesssim 0.93$  GPa and  $1.35 \lesssim p \lesssim 1.36$  GPa. Accordingly, Fig. 1 shows that, at these pressures,  $S_{th}$  decays sharply; the change in  $S_{th}$  being more abrupt for the case of *Ih* than for LDA. The behavior of  $S_{th}$  in Fig. 1 is consistent with the evolution of the tetrahedral order parameter  $q$ <sup>40,41</sup> during the *Ih*-to-HDA and LDA-to-HDA transformations reported in Ref.<sup>39</sup>. In particular, it was found that both *Ih*-to-HDA and LDA-to-HDA transformations occur when the tetrahedral order parameter reaches a specific critical value,  $q \sim 0.32$ . Similarly, Fig. 1 indicates that both transformations occur when  $S_{th}$  reaches the critical value  $S_{th} \sim 0.91$  and  $\sim 0.94$  in LDA and *Ih*, respectively. This strongly suggests that the transformation of LDA and *Ih* to HDA have a common origin, the rearrangement of the HBN<sup>42</sup> that occurs at  $S_{th} \sim 0.91-0.94$ . This also explains why the transformation pressure is higher for *Ih* than for LDA. Specifically, the HBs in *Ih* are more linear (and thus, stronger<sup>22,43</sup>) than in LDA and, hence, in order to distort the HBN to the point that  $S_{th} \sim 0.91-0.94$ , one needs to apply larger pressures to *Ih* than to LDA.

To shed light into the microscopic origin of the LDA-to-HDA and *Ih*-to-HDA transformations, we also study the normalized molecular dipole correlation function,  $C_\mu(p) = \langle \mu(p) \cdot \mu(0) \rangle$ , where  $\mu(0)$  is the molecular dipole vector at pressure  $p = 0$  GPa,  $\mu(p)$  is the molecular dipole vector at pressure  $p$  and  $\langle \cdot \rangle$  indicates a average over all molecules in the system. Figure 2 (a) shows the profile of  $C_\mu(p)$  for the *Ih*-to-HDA transformation (black circles) and for the LDA-to-HDA transformation (red squares).

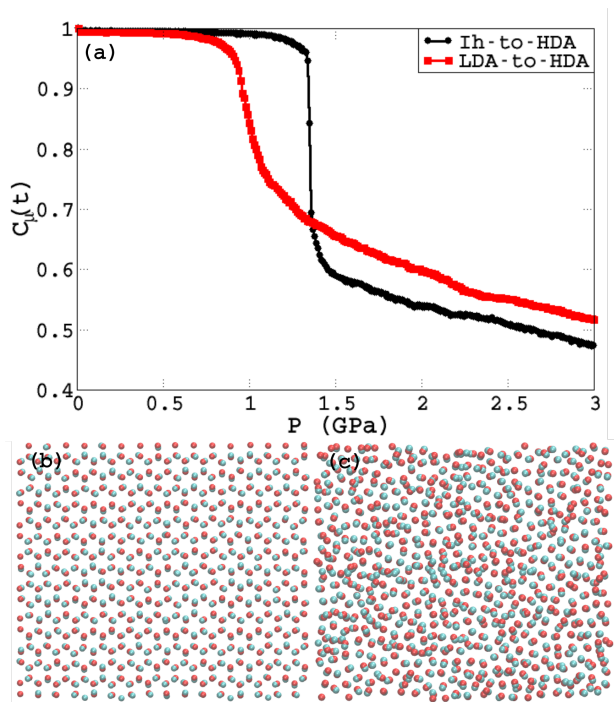


FIG. 2: (a): Water dipole moment correlation function  $C_\mu(p)$  as a function of pressure during the  $Ih$ -to-HDA (black circles) and LDA-to-HDA transformations (red squares). (b): snapshot of a 4 Å-thick slice of  $Ih$  at  $p = 0$  GPa. (c): Snapshot of a 4 Å-thick slice of HDA at  $p = 3.0$  GPa (right). Red spheres represent the oxygen atoms, and the cyan spheres indicate the position of the corresponding dipole end-point.

At low pressures, shows only a mild decay upon compression. In correspondence with both transition pressures,  $C_\mu(p)$  shows a marked drop, indicating that water molecules rotate causing a rearrangement in the HBN. In particular, the drop in  $C_\mu(p)$  for the transformation of  $Ih$  is larger than the drop in  $C_\mu(p)$  for the transformation of LDA. As an example, we include in Fig. 2 (b) and (c) two snapshots of a 4Å-thick slice of  $Ih$  at  $p = 0$  GPa and of HDA at  $p = 3$  GPa. The red spheres correspond to oxygen atoms, while the cyan spheres correspond to the positions of the end-point of the molecular dipoles. One can appreciate how the ordered pattern in the dipoles distribution on  $Ih$  is broken in HDA.

### B. Intermediate-range order: searching for ice $Ih$ , $Ic$ and II-VII

In this section, we focus on the local structure of water at intermediate length scales. Specifically, we study the structure of water during the LDA-to-HDA and  $Ih$ -to-HDA transformations at the level of the second hydration shell. This allows us to compare the structure of LDA and HDA relative to the structure of  $Ih$  as well as intermediate and high-pressure ices. Water can acquire more

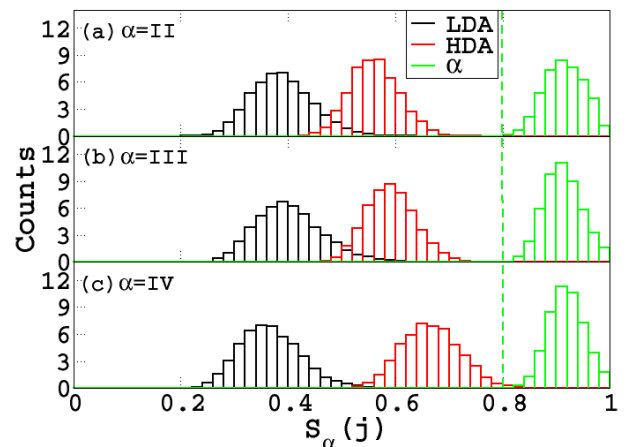


FIG. 3: (a): Histogram of the LOM  $S_\alpha(j)$ , eq. 1 calculated using, as a reference, the unit cells of ice  $\alpha = \text{II}$ , (b):  $\alpha = \text{III}$ , (c)  $\alpha = \text{IV}$  for LDA (black) and for  $\text{HDA}_{Ih}$  (red) at  $p = 0.01$  GPa and at  $p = 3.0$  GPa, respectively. The green distributions represent the histograms for the corresponding bulk ices computed at the following thermodynamic conditions<sup>45</sup>:  $T = 210$  K and  $p = 4$  GPa for ice II, and  $T = 250$  K and  $p = 3$  GPa for ice III and IV. The green line emphasizes the value  $S = 0.8$  used as a cutoff to identify ice-like environments.

than 18 different crystalline forms<sup>44</sup>. However, at the temperature ( $T = 80$  K) and pressures ( $0 \leq p \leq 3$  GPa) studied here, the system can only visit the stability regions of the phase diagram of ice corresponding to  $Ih$  and  $Ic$ , as well as ices II, III, IV, V, VI, VII and VII. Accordingly, we focus on the score function  $S_\alpha$  associated to ice  $\alpha = Ih, Ic, \text{II}, \text{III}, \text{IV}, \text{V}, \text{VI}, \text{VII}$  and VII, and defined using, as a reference structure, the first and/or second hydration shell of the corresponding ice.

Table I shows the value of the score functions  $S_\alpha$  for the cases of LDA at  $p = 0.1$  MPa, and HDA at  $p = 3.0$  GPa. In the case of HDA, we obtain similar values of  $S_\alpha$  for  $\text{HDA}_{LDA}$  and  $\text{HDA}_{Ih}$ . Also included in Table I are the number of crystallites found in LDA and HDA. For a given ice  $\alpha$ , we define a crystallite as a water oxygen  $j$  for which the LOM  $S_\alpha(j) > S_0$ , plus its  $M$  neighbors used in the reference structure of the corresponding LOM.  $S_0$  is a cutoff reference value. In this work, we chose  $S_0 = 0.8$  because we find that, for all ices studied,  $S_\alpha(j) > 0.8$ . As an example, we include in Fig. 3(a)-(c) the probability distribution of  $S_\alpha(j)$  in LDA (black) and HDA (red), for the cases  $\alpha = \text{II}, \text{III}, \text{IV}$ . In Fig. 3(a)-(c) we also report the distributions of  $S_\alpha$  obtained in samples of ice II, III and IV computed in their thermodynamic stability regions (green)<sup>45</sup>. As shown in Table I, these are among the ices with larger values of the score function  $S_\alpha$  in HDA.

There are two main points that follow from our MD simulations. On one hand, (i) LDA and HDA do not contain any crystalline domain, i.e.,  $S_\alpha(j) < 0.8$  for all atoms in

| Ice $\alpha$ | M  | Shells      | $N_{cryst}$ (LDA) | $S_\alpha$ (LDA) | $N_{cryst}$ (HDA) | $S_\alpha$ (HDA) |
|--------------|----|-------------|-------------------|------------------|-------------------|------------------|
| Ih           | 12 | 2nd         | 0                 | 0.416±0.085      | 0                 | 0.581±0.039      |
| Ic           | 12 | 2nd         | 0                 | 0.331±0.081      | 0                 | 0.557±0.039      |
| II           | 11 | 1st and 2nd | 0                 | 0.389±0.054      | 0                 | 0.562±0.049      |
| III          | 11 | 1st and 2nd | 0                 | 0.403±0.015      | 0                 | 0.592±0.054      |
| IV           | 13 | 1st and 2nd | 0                 | 0.368±0.069      | 114±18            | 0.665±0.054      |
| V            | 14 | 1st and 2nd | 0                 | 0.327±0.021      | 0                 | 0.461±0.054      |
| VI           | 11 | 1st and 2nd | 0                 | 0.204±0.033      | 0                 | 0.404±0.054      |
| VII          | 19 | 1st and 2nd | 0                 | 0.312±0.028      | 0                 | 0.469±0.054      |

TABLE I: Score function  $S_\alpha$  (averaged over 10 independent trajectories) for LDA at  $p = 0.1$  MPa and HDA at  $p = 3.0$  GPa.  $S_\alpha$  is the score function defined using, as a reference structure, the first and/or second shell of ice  $\alpha = Ih, Ic, II-VII$ . There are  $M$  water oxygens in these reference structures. Included are the number of crystallites  $N_{cryst}$  found in LDA and HDA for the ices studied (see text).

the systems (in the case of HDA, this holds for HDA prepared by compression of ice *Ih* and LDA). On the other hand, (ii) there are a few spread traces of ice IV in HDA. Specifically, the tail of the distribution of the LOM  $S_{IV}(j)$  for HDA clearly extends to values larger than 0.8 (Fig. 3 (c)), which is not the case of other ices (see, e.g, the cases of ice II and III in Figs.3 (a) and 3 (b)). In particular, the distribution of  $S_{IV}(j)$  in HDA partially overlaps with the corresponding distribution in a pure sample of ice IV. We stress that the number of ice IV-like domains is rather small; there are only 114 ice IV-like centers in HDA at  $p = 3.0$  GPa for the case  $S_0 = 0.8$ . Such molecules have a LOM  $S_{IV}(j) \sim S_0 = 0.8$ , indicating highly distorted environments. The absence of crystallites of ice *Ih*, *Ic* and II-VII and the very small amount of ice IV-like crystallites enable us to conclude that HDA and LDA are indeed true amorphous structures. Our conclusion is strengthened further by inspecting the HBN of the ice IV-like crystallites, as discussed in the next Section.

### 1. Score function based on ice IV

The presence of ice IV-like molecules in HDA is consistent with the crystallization of HDA into ice IV reported in high-pressure experiments<sup>32,33</sup>. Our results also provide support to the hypothesis that HDA may be an intermediate, 'derailed' glassy state formed during the *Ih*-to-ice IV transformation<sup>37</sup>. However, we note that the HBN of the ice IV domains found in HDA differ from the HBN in ice IV. Specifically, the basic structure of ice IV is shown in Fig. 4 and it is characterized by a water hexagon pierced by a donor-acceptor hydrogen bond. This donor-acceptor HB is the origin of the interpenetrating HBN that characterizes ice IV<sup>46</sup>. We have inspected the topology of the HBN of all the 114 ice IV-like domains in HDA at  $p = 3$  GPa and found no indication of the donor-acceptor HB shown in Fig. 4. Hence, the ice IV-like domains should not be interpreted as nanoscopic crystals, but as disordered local domains in which the second shell of neighbors of the central molecule resembles a distorted second hydration shell of ice IV. Indeed,

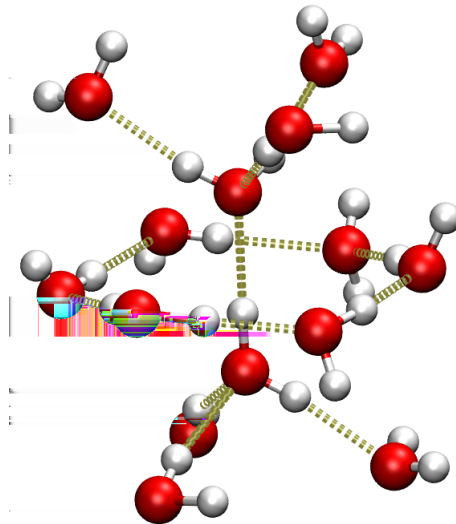


FIG. 4: Unit cell of ice IV. The dashed lines represent the hydrogen bonds.

network interpenetration constrains severely the configurational disorder of water's HBN and is discouraged by entropy. Thus, network interpenetration does not usually occur in disordered structures, such as the amorphous ices. Interestingly, when network interpenetration occurs, HDA does transform into ice IV, as experimentally observed<sup>32,47</sup>. It follows from our results that, although HDA may be considered as a 'derailed' state along the *Ih*-to-IV transformation, the microscopic mechanisms involved in this transformation requires further investigations<sup>37</sup>.

In order to delve deeper into the details of the ice-IV character of HDA, we show in Fig. 5 (a) the pressure-dependence of  $S_{IV}$  during the *Ih*-to-HDA transformation. The  $S_{IV}$  is defined using, as a reference, the unit cell of ice IV shown in Fig. 5 (a). For comparison, we also include  $S_{IV}$  during the LDA-to-HDA transformation. Along both transformations, the ice IV-character of both *Ih* and LDA increases smoothly with pressure and, in correspondence with both non-equilibrium transformations,

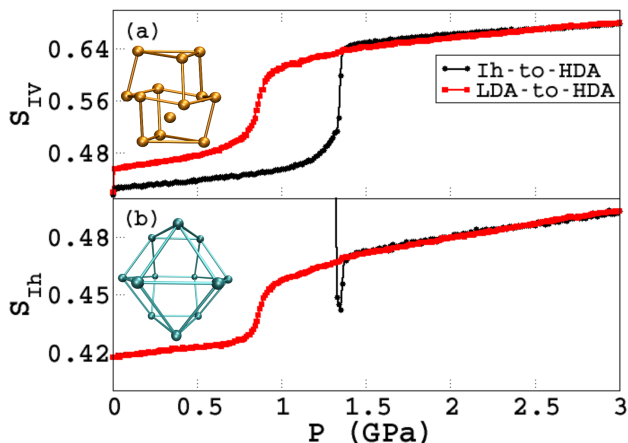


FIG. 5: (a): Score function  $S_{IV}$  during the  $Ih$ -to-HDA (black) and the LDA-to-HDA (red) transformation. The snapshot represents the reference structure used to compute  $S_{IV}$ . (b): Score function  $S_{Ih}$  during the  $Ih$ -to-HDA (black) and the LDA-to-HDA (red) transformation. The snapshot depicts the reference structure used in the definition of  $S_{Ih}$ .

$S_{IV}$  shows a sudden increase, from  $S_{IV} = 0.46 - 0.47$  to  $S_{IV} = 0.64 - 0.66$ . Interestingly, as for the short-range  $S_{th}$ , both  $Ih$  and LDA need to acquire a similar value of  $S_{IV}$  before being converted to HDA, i.e.,  $S_{IV} \sim 0.52$  at the corresponding transition pressures. This observation further explains why the transformation pressure is higher for  $Ih$  than for LDA, and indicates that such difference is an effect that extends also beyond the first hydration shell. We also note that the continuous increment of the ice IV-character with the increasing pressure in HDA is a further indication of the HDA-to-ice IV transformation that may occur at higher pressures<sup>32,33</sup>.

## 2. Score function based on $Ih$

Considering that LDA and  $Ih$  have a similar degree of tetrahedrality (see Fig. 1), one may wonder how similar LDA and  $Ih$  are at the level of the second hydration shell. To address this issue, we study  $S_{Ih}$ , i.e. the score function defined using, as a reference structure, the second hydration shell of ice  $Ih$  (see snapshot of Fig. 5 (b)). Figure 5 (b) shows  $S_{Ih}$  during the  $Ih$ -to-HDA (black line) and LDA-to-HDA (red line) transformations. The values of  $S_{Ih}$  for  $Ih$  at low pressures are not shown because they are, as one would expect, close to 1. Remarkably, in correspondence with the  $Ih$ -to-HDA first-order-like phase transition,  $S_{Ih}$  acquires a minimum that could be interpreted as the limit of mechanical stability for  $Ih$ . Further compression results in a continuous but mild increase in  $S_{Ih}$  within the  $HDA_{Ih}$  state. We note that  $S_{Ih}$  is practically the same for both  $HDA_{LDA}$  and  $HDA_{Ih}$ , indicating that the average structure of HDA is independent of the recipe followed to prepare HDA.

A comparison of Figs. 1 and 5 (b) shows that, although

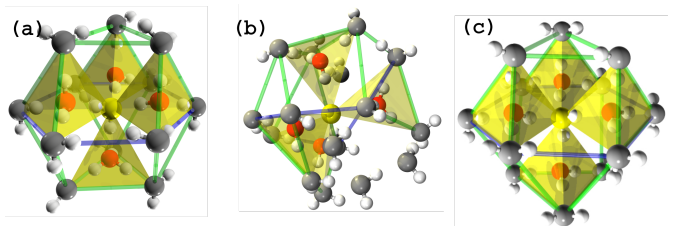


FIG. 6: (a): Local structure of  $Ih$ , (b): LDA, (c): ice Ic. The central water molecule is depicted in yellow and is located at the shared vertex of the four tetrahedra depicted in yellow. The water molecules in the first shell of the central (yellow) water molecule are shown in red and are located at the center of the four (yellow) tetrahedra. The water molecules on the second shell of the central (yellow) molecule are depicted in gray and are located at the outer vertices of the (yellow) tetrahedra. In the case of  $Ih$ , the gray molecules describe an anticuboctahedron whose structure is emphasized by the green and blue lines. In the case of LDA, one of the four (yellow) tetrahedra of the anticuboctahedral cage is broken. In the case of Ic, the second shell of neighbors describes the Archimedean solid cuboctahedron.

LDA and  $Ih$  have very similar tetrahedrality (and density), they differ remarkably at the level of the second shell. This is shown in Fig. 6 (a) and 6 (b) that include, respectively, a representative arrangement of water molecules in the first and second hydration shell of  $Ih$  and LDA, taken from our MD simulations. The yellow water molecule is the shared vertex of four tetrahedra (emphasized in yellow), that are the source of the high tetrahedrality of both samples. The centers of each of these tetrahedra are occupied by the red water molecules; these four (red) water molecules constitute the first hydration shell of the central (yellow) molecule. The outer vertices of the (yellow) tetrahedra are occupied by 12 molecules, shown in gray. These molecules constitute the second hydration shell of the central (yellow) water molecule. The oxygens in the second shell of  $Ih$  describe an anticuboctahedron, emphasized by the blue snapshot in Fig. 5 (b). A comparison of Figs. 6 (a) and (b) shows that, in the local structure of LDA, one of the four tetrahedra is broken, leading to the opening of the anticuboctahedral cage characteristic of  $Ih$ . For comparison, included in Fig. 6 (c) is the local structure of ice Ic. The second shell of neighbors of Ic (gray O atoms) describes the Archimedean solid cuboctahedron<sup>48</sup> and differs from the anticuboctahedron in the local structure of ice  $Ih$ . Specifically, the anticuboctahedron ( $Ih$ ) is the 27<sup>th</sup> Johnson solid<sup>49</sup> and differs from the cuboctahedron (Ic) by a rotation of  $120^\circ$  in one of the four (yellow) tetrahedra (Fig. 6 (c)).

## C. Clustering analysis

In this section, we describe the structural changes underlying the  $Ih$ -to-HDA and the LDA-to-HDA transfor-

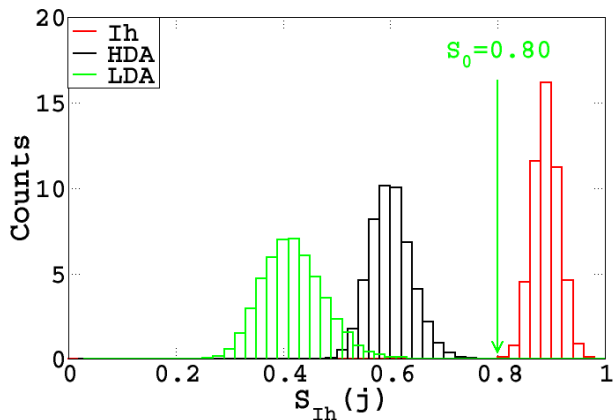


FIG. 7: Histogram of the LOM  $S_{Ih}(j)$  (eq. 1) calculated using, as a reference, the second shell of neighbors of ice  $Ih$  for HDA (black) at  $p = 3.0$  GPa,  $Ih$  (red) at  $p = 0.01$  GPa, and for LDA (green) at  $p = 0.01$  GPa, respectively.

mations by looking at the spatial distribution of ice IV-, ice  $Ih$ -, LDA-, and HDA-like water molecules through the system. We classify a water molecule  $j$  as  $Ih$ -like molecule if the corresponding LOM  $S_{Ih}(j) > S_0$ , and as ice IV-like molecule if its LOM  $S_{IV}(j) > S_0$ ; otherwise, the molecule is considered to belong to an amorphous ice. The value  $S_0 = 0.8$  is chosen because for ices  $\alpha = Ih, IV$ ,  $S_\alpha(j) > 0.8$ , while  $S_\alpha(j) < 0.8$  for molecules in LDA and HDA; see Figs. 7 and 3 (c). In order to distinguish between LDA- and HDA-like molecules, we consider the LOM  $S_{IV}(j)$ . As shown in Fig. 3 (c), molecules in LDA (HDA) are characterized by approximately  $S_{IV}(j) < S_{0'}$  ( $S_{IV}(j) > S_{0'}$ ) with  $S_{0'} = 0.58$ .

This classification of water molecules allows us to identify clusters of LDA, HDA, ice  $Ih$ , and ice IV. Specifically, two molecules, of the same kind (LDA, HDA,  $Ih$ , and IV), are considered to belong to the same cluster if they form a HB. In this work, we consider that two water molecules form a HB if a H atom of one of these molecules is within a distance  $d_{OH} = 2.2$  Å from the O atom of the other molecule; this value of  $d_{OH}$  corresponds to the location of the first minimum in the OH radial distribution function of glassy water at  $p = 3$  GPa (HDA)<sup>42</sup>. With respect to other HB definitions, this definition leads to a fully formed tetrahedral network in LDA and HDA<sup>42</sup>, in agreement with experimental results<sup>50</sup>.

### 1. The $Ih$ -to-HDA transformation

Fig. 8 (a) shows the percentage of  $Ih$ -like (black circles) and HDA-like molecules (red squares) during the  $Ih$ -to-HDA transformation for the pressure window  $0.4 \leq p \leq 1.6$  GPa. Similarly, Fig. 8 (b) shows the percentage of LDA-like molecules (green diamonds) and ice-IV-like molecules (blue triangles) during the same transformation.

At  $p = 0.6$  GPa, the percentage of  $Ih$ -like molecules is large,  $\approx 100\% \approx N$ , and decreases smoothly upon further compression to  $p = 1.34$  GPa. As shown in Figs. 8 (a) and 8 (b), the decrease in  $Ih$ -like molecules is accompanied by an increase in HDA-like molecules, from  $\approx 0\%$  at 0.6 GPa to  $\approx 20\%$  at  $p = 1.34$  GPa. We note that, at these pressures, the percentage of LDA-like molecules is relatively small ( $\sim 1\%$ ) and it reaches a maximum at  $p = 1.1 - 1.2$  GPa, while there are no ice IV-like molecules (at  $p < 1.34$  GPa). In correspondence with the  $Ih$ -to-HDA transformation at  $p = 1.35$  GPa, we observe a significant drop in the percentage of  $Ih$ -like molecules, from  $\approx 80\%$  to  $\approx 20\%$  which is accompanied by an increase in the number of HDA-like molecules, from  $\approx 20\%$  to  $\approx 80\%$ . Such increment involves also the transformation of LDA domains into HDA domains, accounting for the decrease of LDA domains occurring at lower pressures. Interestingly, at  $p > 1.35$  GPa, HDA contains a small number of residual, LDA and IV molecules; e.g., at  $p = 1.4$  GPa, there are only  $\approx 0.03\%$  molecules of LDA and ice IV. In addition, depending on pressure, specifically  $HDA_{Ih}$  may also contain non-negligible amounts of residual ice  $Ih$  molecules. At  $p = 1.6$  GPa, there is an amount of  $\sim 3.5\%$  of  $Ih$ -like molecules while ice  $Ih$  molecules are absent at  $p = 3$  GPa.

Figures. 8 (c) and 8 (d) show the percentage of clusters associated to LDA, HDA, ice  $Ih$  and IV. At pressures below the transformation pressure, the system contains only one  $Ih$ -cluster with several, small disconnected HDA-like and LDA-like clusters. Indeed, the largest LDA- and HDA-cluster are composed by  $< 0.1\%$  of the total number of molecules (at  $p < 1.34$  GPa) (Fig.8 (f) and 8 (e)). On the other hand, in correspondence with the  $Ih$ -to-HDA transformation, the number of  $Ih$ -like clusters increases, from  $\sim 0.1\%$  to  $\approx 3\%$ , while the number of HDA-clusters reduces to  $\sim 0.1\%$ . As shown in Fig. 8 (e), the largest HDA-cluster has  $\approx 98\%$  molecules and hence, it includes most of the molecules in the system while, instead, the largest  $Ih$ -cluster is small ( $\sim 0.1\%$  molecules in size) and therefore, they are within the HDA matrix. In Fig. 9 we show a zoom of the percentage of the largest  $Ih$ - and of the HDA-clusters as a function of the pressure. It is possible to observe that the largest  $Ih$ -cluster shrinks at a faster pace of which the corresponding HDA-cluster increases, indicating that most of the HDA-like domains formed upon increasing the pressure, do not populate the largest HDA-cluster but, rather, are dispersed on the  $Ih$  sea. It follows that the  $Ih$ -to-HDA transformation is reminiscent of a transformation driven by a spinodal decomposition, rather than by a nucleation-and-growth process as found during crystallization.

### 2. The LDA-to-HDA transformation

A similar picture holds for the LDA-to-HDA transformation. However, in this case, the transformation is smoother and there are no  $Ih$ -like molecules at any pres-



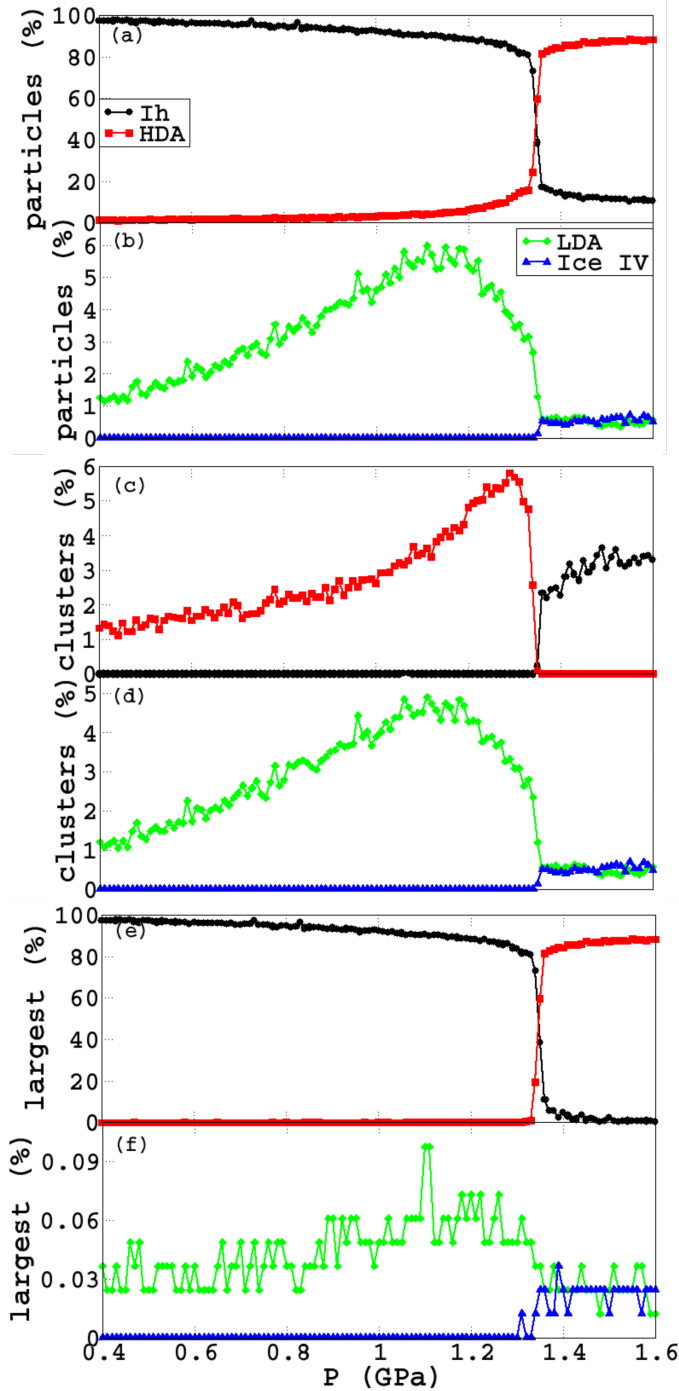


FIG. 8: (a)-(b): Percentage of *Ih*- (black circles) and HDA-like (red squares) molecules, and LDA- (green diamonds) and ice IV-like (blue triangles) molecules during the *Ih*-to-HDA transformation. The corresponding percentage of clusters are indicated in (c) and (d). (e)-(f) show the percentage of molecules composing the ice *Ih*-, ice IV-, LDA-, and HDA-clusters.

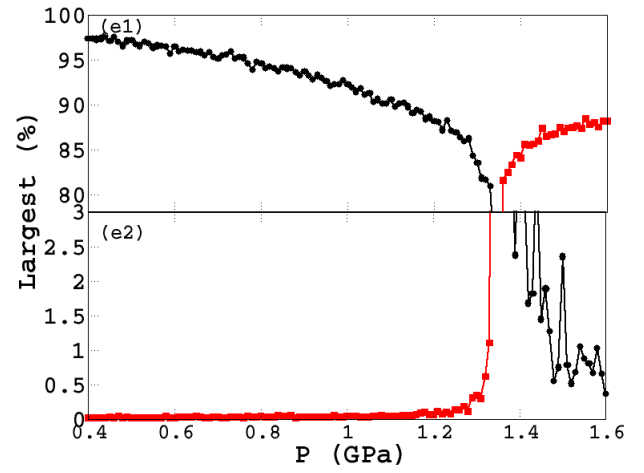


FIG. 9: (e1): Percentage of molecules composing the ice *Ih*- and HDA-clusters in the size window 80% – 100%. (e2): Percentage of molecules composing the ice *Ih*- and HDA-clusters in the size window 0% – 3%.

sure. Accordingly, we only discuss the roles of LDA and HDA during the LDA-to-HDA transformation.

Fig. 10 (a) shows the percentage of LDA-like (black circles) and HDA-like molecules (red squares) during the LDA-to-HDA transformation for the pressure window  $0.01 \leq p \leq 1.2$  GPa. At  $p = 0.01$  GPa, the percentage of LDA-like molecules is large,  $\approx 95\%$ , and decreases smoothly upon further compression to  $p = 0.8$  GPa. As shown in Figs. 10 (a), the decrease in HDA-like molecules is accompanied by an increase in HDA-like molecules, from  $\approx 10\%$  at  $p \sim 0$  GPa to  $\approx 30\%$  at  $p = 0.80$  GPa. In correspondence with the onset of the LDA-to-HDA transformation at  $p = 0.80$  GPa, we observe a significant drop in the number of LDA-like molecules, from  $\approx 70\%$  to  $\approx 20\%$  at  $p = 0.9$  GPa, which is accompanied by an increase in the number of HDA-like molecules, from  $\approx 20\%$  to  $\approx 80\%$ .

Figure 10 (b) shows the percentage of clusters associated to LDA and HDA. At pressures below the transformation pressure, the system contains one LDA-cluster with several, small disconnected HDA-like clusters that increase in number upon compression, reaching a maximum of  $\sim 10\%$  clusters at  $p \sim 0.7$  GPa. The largest HDA-cluster at  $p < 0.8$  GPa is composed by less than 0.1% of the total number of molecules; see Fig. 10 (c). On the other hand, in correspondence with the pressure window  $0.8 \lesssim p \lesssim 1.0$  GPa, the number of LDA-like clusters increases, from  $\approx 1\%$  to  $\approx 9\%$  and they decrease at higher pressures, while the percentage of HDA-clusters reduces to almost zero. At  $p > 0.9$  GPa, this HDA-cluster has  $N \sim 98\%$  of the total number of molecules in the system while, instead, the largest LDA-cluster is small ( $< 0.1\%$  molecules in size) and therefore, they are within the HDA matrix. It follows that, in analogy with the *Ih*-to-HDA transformation, the LDA-to-HDA transformation is reminiscent of a transformation driven by

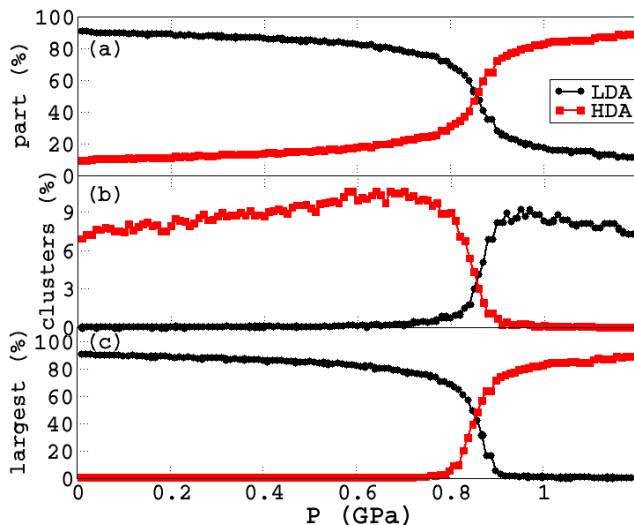


FIG. 10: (a): Percentage of LDA and HDA environments in black and red, respectively for the LDA-to-HDA transformation. (b): Percentage of number of clusters and (c): of the largest LDA and HDA clusters (lower panel).

spinodal decomposition.

#### IV. SUMMARY AND CONCLUSIONS

We performed classical MD simulations and explored in detail the structure of water at short and intermediate scales during the LDA-to-HDA and *Ih*-to-HDA transformations. Specifically, by using the LOM developed in Ref.<sup>34</sup>, we searched for locally ordered crystalline domains composed by the first and/or second shell of neighbors in the amorphous ices formed during the *Ih*-to-HDA and the LDA-to-HDA pressure-induced transformations. Our results confirm that LDA and HDA are indeed amorphous, i.e., they lack of polydispersed ice-like structures. Surprisingly, we find that HDA contains a small number of domains that are reminiscent of ice IV. The presence of ice IV-like domains provides some support to the hypothesis that HDA could be a 'derailed' state along the *Ih*-to-ice IV pathway<sup>37</sup>. However, the HBN of these domains differ from the HBN of ice IV. The ice IV basic structure includes the interpenetration of two HBN (Fig. 4). However, interpenetration of HBNs is highly improbable in amorphous structures such as HDA since it constrains the local possible orientations of water molecules and hence, it tends to reduce the entropy of the amorphous ice. In our view, since the crystallization to ice IV has been shown to have the lowest activation energy out of all of the possible crystallization pathways around 1 GPa<sup>32,33,47</sup>, the transformation of HDA to ice IV is not fully understood and requires further investigation.

By characterizing the structure of water at the first and second hydration shells, we also provided some understanding of the differences and similarities in the molecu-

lar changes underlying the LDA-to-HDA and *Ih*-to-HDA transformations. Our results indicate that both nonequilibrium transformations are two-steps processes where, first, a small distortion of the HBN occurs at low pressures and then, a sudden, extensive re-arrangement of HBs at the corresponding transformation pressure occurs. The *Ih*-to-HDA and LDA-to-HDA transformations occur when LDA and *Ih* have similar local order, as quantified by various score functions (e.g.,  $S_{IV}$ ,  $S_{Ih}$ , and  $S_{th}$ ). Since *Ih* has a perfect tetrahedral HBN, while LDA does not, it follows that higher pressures are needed to distort the HBN of *Ih* relative to LDA. Accordingly, *Ih* can resist larger pressures than LDA before collapsing to HDA, as found in experiments<sup>30,31</sup>.

From the microscopic point of view, *Ih* and LDA are structurally similar at small length-scales, both being characterized by a nearly perfect regular tetrahedral HBN. Yet, the *Ih*-to-HDA transformation is sharp while the LDA-to-HDA transformation is gradual. Our results suggest that the gradualness of the LDA-to-HDA transformation is due to different structural configurations occurring at the level of the second shell of neighbors: *Ih* has a well-formed anticuboctahedral structure and an ordered HBN (which rearranges rapidly upon compression for this water model), while LDA has an open cage that causes some degree of disorder in the HBN (Fig. 6) (and rearranges more gradually upon compression)<sup>42</sup>.

We also find that both *Ih*-to-HDA and LDA-to-HDA transformations are first-order-like phase transitions occurring via spinodal decomposition in which HDA clusters percolate within the *Ih*/LDA sample. At pressures below the *Ih*/LDA-to-HDA transformations, the system consists of a single large cluster of *Ih*/LDA, composed by most of the molecules in the system, plus HDA clusters, composed of few water molecules. At pressures above the transformation pressure, the roles of HDA and *Ih*/LDA are inverted, i.e., the system is composed of a single HDA-cluster composed by most of the molecules in the system, and *Ih*/LDA clusters (depending on whether the starting phase is *Ih* or LDA) that are composed by a few water molecules.

We conclude by noting that  $HDA_{Ih}$  and  $HDA_{LDA}$ , at  $p = 3$  GPa, are practically identical in terms of water structure at the first- and second-hydration shells. However, minor differences in structure seem to exist at lower pressures, closer to the collapse of *Ih* and LDA to HDA. For example, it follows from Fig. 8(a) that  $HDA_{Ih}$  contains a few, non-negligible number of *Ih*-like molecules at  $p \sim 1.4 - 1.6$  GPa while, not surprisingly,  $HDA_{LDA}$  does not. This is consistent with the picture proposed in Refs.<sup>5,6</sup> where uHDA (at  $p < 1.5$  GPa) is considered to contain *Ih* crystallites while other HDA forms, such as eHDA, do not. In our case,  $HDA_{Ih}$  is prepared following the same protocol followed in experiments to prepare uHDA and, accordingly, it contains ice *Ih* at  $p \sim 1.5$  GPa. Instead,  $HDA_{LDA}$  does not contain ice *Ih*, as is the case of eHDA. In the pressure range  $1.4 \lesssim p \lesssim 1.6$  GPa, the *Ih*-clusters in  $HDA_{Ih}$  are small, composed by  $< 5 - 10$

molecules.

Our results shed light on the debated structural properties of amorphous ices and indicate that the kinetics of the *Ih*-to-HDA and LDA-to-HDA transformations requires an in depth inspection of the underlying HBN. Such investigation is currently ongoing and will be the subject of a forthcoming publication<sup>42</sup>.

### Acknowledgments

This work was supported by the STFC Hartree Centre's Innovation Return on Research programme, funded

by the Department for Business, Energy & Industrial Strategy. This work was partially supported by the National Science Foundation (CBS-1604504 award to NG) and a grant of computer time from the City University of New York High Performance Computing Center under NSF Grants CNS-0855217, CNS-0958379 and ACI-1126113. R. C. acknowledges partial support from the U.S. Department of Energy under award No. DE-SC0008626. S. T. was supported by the National Science Foundation under Award No. DMR1714722.

- 
- <sup>1</sup> P. G. Debenedetti. Supercooled and glassy water. *J. Phys.: Condens. Matter*, 15:R1669, 2003.
  - <sup>2</sup> C. A. Angell. Amorphous water. *Annu. Rev. Phys. Chem.*, 55:559, 2004.
  - <sup>3</sup> T. Loerting and N. Giovambattista. Amorphous ices: experiments and numerical simulations. *J. Phys.: Condens. Matter*, 18:R919, 2006.
  - <sup>4</sup> O. Mishima and H. E. Stanley. The relationship between liquid, supercooled and glassy water. *Nature*, 396:329, 1998.
  - <sup>5</sup> T. Loerting, V. Fuentes-Landete, P. H. Handlea, M. Seidl, K. Amann-Winkel, C. Gainaru, and R. Bohme. The glass transition in high-density amorphous ice. *J. Non-Cryst. Solids*, 407:423430, 2015.
  - <sup>6</sup> K. Amann-Winkel, R. Bohmer, F. Fujara, C. Gainaru, B. Geil, and T. Loerting. Colloquium: Waters controversial glass transitions. *Rev. Mod. Phys.*, 88:011002, 2016.
  - <sup>7</sup> E. Meyer. New method for vitrifying water and other liquids by rapid cooling of their aerosols. *J. Appl. Phys.*, 58:663, 1985.
  - <sup>8</sup> E. F. Burton and W. F. Oliver. *Nature*, 135:505, 1935.
  - <sup>9</sup> P. Jenniskens and D. F. Blake. Structural transitions in amorphous water ice and astrophysical implications. *Science*, 265:753, 1994.
  - <sup>10</sup> O. Mishima. Reversible first-order transition between two h<sub>2</sub>o amorphs at  $\sim 0.2$  gpa and  $\sim 135$  k. *J. Chem. Phys.*, 100:5910, 1994.
  - <sup>11</sup> O. Mishima, L. D. Calvert, and E. Whalley. 'melting ice' i at 77 k and 10 kbar: a new method of making amorphous solids. *Nature*, 310:393–395, 1984.
  - <sup>12</sup> O. Andersson. Glass-liquid transition of water at high pressure. *Proc. Natl. Acad. Sci. USA*, 108:11013–11016, 2011.
  - <sup>13</sup> T. Loerting, W. Schustereder, K. Winkel, C. G. Salzmann, I. Kohl, , and E. Mayer. Amorphous ice: Stepwise formation of very-high-density amorphous ice from low-density amorphous ice at 125 k. *Phys. Rev. Lett.*, 96:025702, 2006.
  - <sup>14</sup> K. Winkel, M. Bauer, E. Mayer, M. Seidl, M. S. Elsaesser, and T. Loerting. Structural transitions in amorphous h<sub>2</sub>o and d<sub>2</sub>o: the effect of temperature. *J. Phys.: Condens. Matter*, 20:494212, 2008.
  - <sup>15</sup> K. Winkel, E. S. Elsaesser, E. Mayer, , and T. Loerting. Water polymorphism: Reversibility and (dis)continuity. *J. Chem. Phys.*, 128:044510, 2008.
  - <sup>16</sup> K. Winkel, E. Mayer, and T. Loerting. Equilibrated high-density amorphous ice and its first-order transition to the low-density form. *J. Phys. Chem. B*, 115:14141–14148, 2011.
  - <sup>17</sup> E. L. Gromnitskaya, O. V. Stal'gorova, V. V. Brazhkin, and A. G. Lyapin. Ultrasonic study of the nonequilibrium pressure-temperature diagram of h<sub>2</sub>o ice. *Phys. Rev. B*, 64:094205, 2011.
  - <sup>18</sup> T. Loerting, C. Salzmann, I. Kohl, E. Mayer, and A. Hallbrucker. A second distinct structural state of high-density amorphous ice at 77 k and 1 bar. *Phys. Chem. Chem. Phys.*, 3:5355–5357, 2001.
  - <sup>19</sup> K. Winkel, D. T. Bowron, T. Loerting, E. Mayer, and J. L. Finney. Relaxation effects in low density amorphous ice: Two distinct structural states observed by neutron diffraction. *J. Chem. Phys.*, 130:204502, 2009.
  - <sup>20</sup> R. J. Nelmes, J. S. Loveday, T. Strässle, C. L. Bull, M. Guthrie, G. Hamel, and S. Klotz. Annealed high-density amorphous ice under pressure. *Nature Phys.*, 2:414, 2006.
  - <sup>21</sup> T. Loerting, K. Winkel, M. Bauer, C. Mitterdorfer, P. H. Handle, E. Mayer, J. L. Finney, and D. Bowron. How many amorphous ices are there? *Phys. Chem. Chem. Phys.*, 13:8783–8794, 2011.
  - <sup>22</sup> B. Santra, R. A. DiStasio Jr., F. Martelli, and R. Car. Local structure analysis in ab initio liquid water. *Mol. Phys.*, 113:2829–2841, 2015.
  - <sup>23</sup> C. A. Tulk, C. J. Benmore, L. Urquidi, D. D. Klug, J. Neuefeing, B. Tomberli, and P. A. Egelstaff. Structural studies of several distinct metastable forms of amorphous ice. *Science*, 297:1320–1323, 2002.
  - <sup>24</sup> J. L. Finney, A. Hallbrucker, I. Kohl, A. K. Soper, and D. T. Bowron. Structures of high and low density amorphous ice by neutron diffraction. *Phys. Rev. Lett.*, 88:225503, 2002.
  - <sup>25</sup> A. K. Soper and M. A. Ricci. Structures of high-density and low-density water. *Phys. Rev. Lett.*, 84:2881, 2000.
  - <sup>26</sup> J. Wong, D. A. Jahn, and N. Giovambattista. Pressure-induced transformations in glassy water: A computer simulation study using the tip4p/2005 model. *J. Chem. Phys.*, 143:074501, 2015.
  - <sup>27</sup> R. Martoňak, D. Donadio, and M. Parrinello. Evolution of the structure of amorphous ice: From low-density amorphous through high-density amorphous to very high-density amorphous ice. *J. Chem. Phys.*, 122:134501, 2005.
  - <sup>28</sup> F. Martelli, S. Torquato, N. Giovambattista, and R. Car. Large-scale structure and hyperuniformity of amorphous

- ices. Phys. Rev. Lett., 119:136002, 2017.
- <sup>29</sup> J. S. Tse, D. D. Klug, C. A. Tulk, I. Swainson, E. C. Sensson, C.-K. Loong, V. Shapakov, V. R. Belosludov, R. V. Belosludov, and Y. Kawazoe. The mechanism of pressure-induced amorphization of ice ih. Nature, 400:647–649, 1999.
- <sup>30</sup> G. P. Johari. On the amorphization of hexagonal ice, the nature of water’s low-density amorph, and the continuity of molecular kinetics in supercooled water. Phys. Chem. Chem. Phys., 2:1567–1577, 2000.
- <sup>31</sup> G. P. Johari and O. Andersson. Mechanisms for pressure- and time-dependent amorphization of ice under pressure. Phys. Rev. B, 70:184108, 2004.
- <sup>32</sup> C. G. Salzmann, T. Loerting, T. Kohl, E. Mayer, and A. Hallbrucker. Pure ice iv from high-density amorphous ice. J. Phys. Chem. B, 106:5587–5590, 2002.
- <sup>33</sup> C. G. Salzmann, E. Mayer, and A. Hallbrucker. Effect of heating rate and pressure on the crystallization kinetics of high-density amorphous ice on isobaric heating between 0.2 and 1.9 gpa. Phys. Chem. Chem. Phys., 6:5156–5165, 20024.
- <sup>34</sup> F. Martelli, H.-Y. Ko, E. C. Oğuz, and R. Car. Local-order metric for condensed phase environments. Phys. Rev. B, 97:064105, 2016.
- <sup>35</sup> F. Martelli, H.-Y. Ko, C. C. Borallo, and G. Franzese. Structural properties of water confined by phospholipid membranes. Front. Phys., 13:136801, 2018.
- <sup>36</sup> B. Santra, H.-Y. Ko, Y. W. Yeh, F. Martelli, I. Kaganovich, Y. Raitses, and R. Car. Root-growth of boron nitride nanotubes: Experiments and *Ab Initio* simulations. arXiv:1803.11374 [physics.chem-ph], 2018.
- <sup>37</sup> J. J. Shephard, S. Ling, G. C. Sosso, A. Michaelides, B. Slater, and C. G. Salzmann. Is high-density amorphous ice simply a ”derailed” state along the ice i to ice iv pathway? J. Phys. Chem. Lett., 8:1645–1650, 2017.
- <sup>38</sup> J. L. F. Abascal and C. Vega. Pressure-induced transformations in glassy water: A computer simulation study using the tip4p/2005 model. J. Chem. Phys., 123:234505, 2005.
- <sup>39</sup> J. Engstler and N. Giovambattista. J. Chem. Phys., Heating- and pressure-induced transformations in amorphous and hexagonal ice: A computer simulation study using the TIP4P/2005 model:074505, 2017.
- <sup>40</sup> P.-L. Chau and J. Hardwick. A new order parameter for tetrahedral configurations. Mol. Phys., 93:511–518, 1998.
- <sup>41</sup> J. R. Errington and P. G. Debenedetti. Relationship between structural order and the anomalies of liquid water. Nature, 409:318–321, 2001.
- <sup>42</sup> F. Martelli and N. Giovambattista. In preparation.
- <sup>43</sup> B. Santra, J. Klimeš, D. Alfé, A. Tkatchenko, B. Slater, A. Michaelides, R. Car, and M. Scheffler. Hydrogen bonds and van der waals forces in ice at ambient and high pressures. Phys. Rev. Lett., 107:185701, 2011.
- <sup>44</sup> T. Bartles-Rausch, V. Bergeron, J. H. E. Cartwright, R. Escribano, J. L. Finney, H. Grothe, P. J. Gutierrez, J. Haapala, W. F. Fuchs, J. B. C. Pettersson, S. D. Price, C. I. Sainz-Daz, D. J. Stokes, G. Strazzulla, E. S. Thomson, H. Trinks, and N. Uras-Aytemiz. Ice structures, patterns, and processes: A view across the icefields. Rev. Mod. Phys., 84:885–994, 2012.
- <sup>45</sup> M. M. Conde, M. A. Gonzalez, J. F. L. Abascal, and C. Vega. Determining the phase diagram of water from direct coexistence simulations: The phase diagram of the tip4p/2005 model revisited. J. Chem. Phys., 139:154505, 2013.
- <sup>46</sup> H. Engelhardt and B. Kamb. Structure of ice iv, a metastable high-pressure phase. J. Chem. Phys., 48:5887–5899, 1981.
- <sup>47</sup> C. G. Salzmann, I. Kohl, T. Loerting, E. Mayer, and A. Hallbrucker. Pure ices iv and xii from high-density amorphous ice. Can. J. Phys., 81:25–32, 2003.
- <sup>48</sup> P. R. Cromwell. Polyhedra. New York: Cambridge University Press, 1999.
- <sup>49</sup> N. W. Johnson. Convex polyhedra with regular faces. Canad. J. of Math., 18:169, 1966.
- <sup>50</sup> C. Lin, J. S. Smith, S. V. Sinogeikin, and G. Shen. Experimental evidence of low-density liquid water upon rapid decompression. Proc. Natl. Acad. Sci. U.S.A., 2018.